ELSEVIER

Atmospheric Research 52 (1999) 143–165

ATMOSPHERIC RESEARCH

www.elsevier.com/locate/atmos

Evolution of small cumulus clouds in Florida: observations of pulsating growth

Jeffrey R. French *, Gabor Vali, Robert D. Kelly

Department of Atmospheric Science, University of Wyoming, PO Box 3038, Laramie, WY 82071, USA

Received 1 February 1999; accepted 24 March 1999

Abstract

Observations have been made in six small cumulus clouds using instrumented aircraft, a ground-based radar, and a 95 GHz airborne Doppler radar. The clouds occurred on two days during the Small Cumulus Microphysics Study in east-central Florida, summer 1995. Cloud tops were below 3 km and in-cloud temperatures were warmer than 10°C. Maximum observed reflectivity factors were less than 0 dBZ. The evolution of the kinematics of the observed clouds was tracked using measurements from both radars. High-resolution cross-sections of reflectivity and vertical Doppler velocity from the airborne radar appear remarkably similar to fine-scale models of convection reported in the literature. In general, each cloud resembled a collection of individual bubbles ascending through the boundary layer. During the growth phase of a bubble, a positive correlation existed between vertical velocity and reflectivity. As bubbles penetrated further into the inversion, entrainment/detrainment led to a weakening or, in some cases, a reversal of this correlation. Growth of subsequent bubbles ascending through remnants of earlier bubbles were aided by an increase in the amount of moisture in the environment resulting from earlier detrainment of cloudy air, and thus were able to achieve higher altitudes than their predecessors.

Keywords: Cumulus; Convection; Kinematics; Radar

1. Introduction

The early evolution of cumulus clouds is often modeled as the growth of multiple bubbles rising through the convective boundary layer (Mason and Jonas, 1974;

* Corresponding author. Fax: +1-307-766-2635; E-mail: french@grizzly.uwyo.edu

0169-8095/99/$ - see front matter
PII: S0169-8095(99)00024-1

Roesner et al., 1990). Such models have been developed to match calculations of parameters such as liquid water content and moments of droplet distributions with in situ observations. While these models are able to explain the general characteristics of observed clouds, they remain fairly crude and are not able to capture the high degree of variability normally observed in cumuli. Models of cumulus growth such as those from Klaassen and Clark (1985) and Grabowski (1993) more resemble laboratory experiments of convection (e.g., Johari, 1992). These models depict cumulus growth as discrete thermals disconnecting themselves from the surface layer. As they rise, entrainment/detrainment leads to very complex structures within the vertical velocity and cloud liquid water fields. Again, this matches to some degree with in situ measurements, but it has not been fully borne out by observations.

Results from past observational studies of the development of drizzle and the role of entrainment/detrainment in the evolution of cumulus clouds tend to oversimplify the kinematics of such clouds. Much of this work is based exclusively on measurements made from cloud penetrating aircraft (e.g., Austin et al., 1985; Blyth and Latham, 1985; Jonas, 1990). Collecting a set of comprehensive observations in small cumuli with an aircraft is quite difficult because of the highly transient nature of these clouds. In situ measurements, while providing high resolution, sample only along a line through a cloud. Successive penetrations may be separated by several minutes. Even for cases when two aircraft are making simultaneous penetrations at different levels (e.g., Barnes et al., 1996) it is still difficult to extract more than a crude understanding of the kinematics. Even this requires an assumption of a low degree of spatial and temporal variation.

Ground-based Doppler radars provide samples of entire cloud volumes at reasonably high temporal resolution. Based on a series of critical assumptions, the vertical velocity field within clouds may be deduced. The evolution of kinematics can then be determined from measurements of the reflectivity and deduced vertical velocity fields. While this process has had success for larger convective systems (e.g., Szumowski et al., 1997) it is much more difficult to apply to smaller clouds. Further reducing the effectiveness of ground-based radars is the effect of Bragg scattering within weak radar echoes. Knight and Miller (1993) demonstrated that echoes less than roughly -10 dBZ_e and $+10$ dBZ_e for measurements made at 3 and 10 cm, respectively, may contain significant signal due to Bragg scatter. Interpretation of the microphysics from very early, relatively weak radar signals is therefore quite difficult. For studying the very early stages of cumulus growth larger ground-based radars are a necessary tool to augment data from other instruments, but are of limited use when the data are used independently.

Shorter wavelength (specifically K_a-band and W-band) airborne Doppler radars begin to bridge the gap between aircraft in situ observations and measurements from ground-based radars. In general they provide high spatial resolution. Bragg scatter does not affect measurements from such radars. Also, if operating in a vertically pointing mode, they can resolve the vertical Doppler velocity field in addition to the reflectivity. Of course, if mounted on aircraft, the temporal resolution is still rather low, requiring additional measurements from a ground-based radar. Finally, additional in situ measurements along the flight path add information necessary for microphysical interpretation of reflectivity measurements. Ideally, to describe the kinematic evolution of small cumuli

requires measurements from a ground-based radar, a high frequency airborne Doppler radar, and at least one, preferably more than one, cloud penetrating aircraft.

This paper addresses the morphology of small, warm cumulus clouds observed simultaneously with a ground-based and an airborne Doppler radar. French et al. (1999), hereafter referred to as F99, utilized this same data set and drew heavily on in situ measurements to explore the microphysical structure and evolution of such clouds. This paper focuses on the development and evolution of the Rayleigh reflectivity echo and its relationship to the kinematic structure of the clouds investigated in F99. In particular, the pulsating nature of growth of these clouds is discussed. Evidence is presented of the importance of multiple bubbles in cloud evolution. In doing so, data from two radars are used to identify and track bubbles as they ascend.

2. Data set

The data were collected during the Small Cumulus Microphysics Study (SCMS) in east central Florida, USA, summer, 1995. Observations are from measurements made in 6 clouds on two days (5 August and 7 August). The clouds were quite small, typical diameters were less than 2 km. Maximum cloud depth was roughly 2.5 km and fully contained below the 0°C isotherm. Lifetimes of individual clouds were on the order of 30 min.

Instruments utilized for this study include two cloud radars and three cloud penetrating aircraft. The National Center for Atmospheric Research (NCAR) CP-2 radar operated simultaneously in the X-band and S-band providing measurements of the total equivalent reflectivity at both wavelengths. From this, estimates were made of both the Bragg and Rayleigh scatter components of the reflectivity echo. A 95 GHz airborne Doppler radar operated by the University of Wyoming (UW) and mounted on the UW King Air cloud penetrating aircraft provided high resolution, essentially instantaneous, cross-sections of the Rayleigh reflectivity factor and Doppler velocity. Along with the aforementioned King Air, the NCAR C130 and Meteo-France Merlin made measurements of pertinent cloud physical parameters including, but not limited to, cloud liquid water content, hydrometeor size distributions, and three-dimensional air velocities.

2.1. CP-2 measurements

CP-2 was located on a thin strip of land separating the Indian River and Mosquito Lagoon on the northwest end of Kennedy Space Center (KSC). Due to ground clutter considerations, airspace restrictions, and sensitivity requirements, the target area was primarily restricted to the southeast quadrant, 5 to 20 km from the radar (Fig. 1). Clouds were scanned continuously through a series of fixed-azimuth scans (RHIs) separated by 1 to 1.5 degrees. Complete volume scans required roughly 2 to 2.5 min to complete and covered between 20 to 30° in azimuth. Range gates were spaced at 100 m and the across beam resolution was slightly better than 1°.

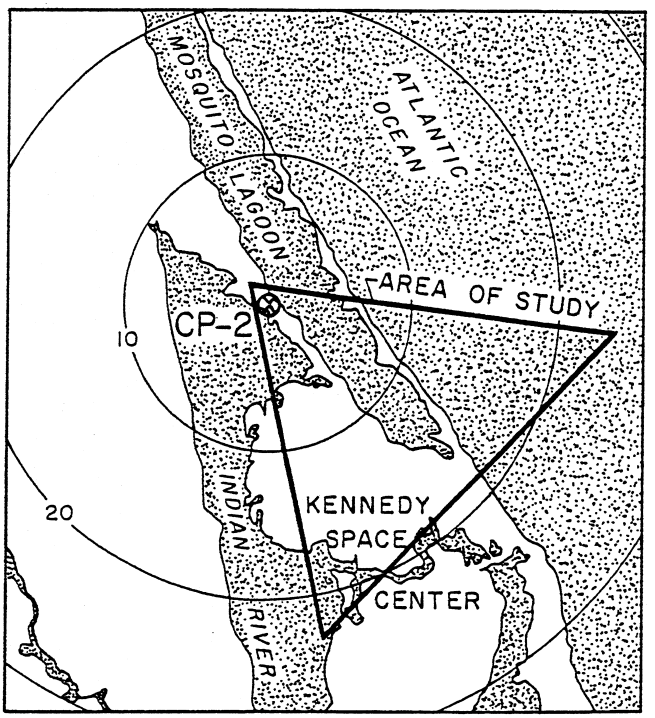

Fig. 1. Map showing the location of the CP-2 radar site and selected range rings (km). The triangle indicates the primary study area for SCMS.

2.1.1. Scattering mechanisms

The Rayleigh reflectivity factor (hereafter referred to as Z_R) results from scattering due to spherical particles for which the Rayleigh approximation is valid (i.e., Doviak and Zrnic, 1984). Sharp gradients in index of refraction due to inhomogeneities in the water vapor field near the edges of rising thermals may lead to 'angel echoes' (Atlas, 1959). Such echoes are due to Bragg scattering which result from the scattering of radiation incident upon dielectric fluctuations located at roughly one-half the radar wavelength. Knight and Miller (1993) illustrated that for weak radar echoes such as those observed in this study, there may be a significant contribution to the total reflectivity due to Bragg scattering. Interpretation of reflectivity echoes then becomes ambiguous if both the Bragg and Rayleigh components contribute significantly to the total backscatter.

Measurements of the water equivalent radar reflectivity factor made simultaneously at X-band and S-band (hereafter referred to as Z_X and Z_S) were used to separate the Bragg and Rayleigh components of the backscattered signal. The algorithm, described most recently by Knight and Miller (1998), requires the common assumption that the dielectric fluctuations at centimeter scales that give rise to the Bragg echo are within the inertial sub-range. Given this, the power spectral density is then related to the wavelength of the fluctuations through a $-5/3$ power law (Ottersten, 1969). Thus, measure-

ments provided by CP-2 of pure Bragg scatter would result in a difference in the back-scattered signal at the two wavelengths of roughly 19 dB.

2.1.2. Echo interpretation

Measurements made at X-band are more sensitive to the Rayleigh component of the equivalent reflectivity factor than those at S-band. To interpret the radar returns, it is useful to construct a series of limits. If either the Rayleigh or Bragg component is greater than the other by a given amount (for this purpose we arbitrarily choose 5 dB), we conclude that the larger of the two dominates the reflectivity. Table 1 illustrates which component dominates at either wavelength for different values of $Z_S - Z_X$. For differences less than 13 dB, Rayleigh scattering dominates Z_X. It is not until differences are greater than 18 dB that Bragg scattering dominates at X-band. For differences between 13 and 18 dB, the Bragg and Rayleigh components are within 5 dB of each other and this type of interpretation becomes ambiguous. Conversely, Bragg scatter generally dominates Z_S unless differences are less than 6 dB. Also, it is not until differences are less than 3 dB that Rayleigh scattering dominates at both wavelengths.

2.1.3. Uncertainties in determining Z_R

A number of uncertainties in estimating Z_R arise from hardware calibration considerations, incomplete or invalid assumptions, and the nature of the algorithm itself. Such factors as beam mismatch, relative calibration between the two channels, and the presence of non-Rayleigh scatterers are discussed in some detail in (Knight and Miller, 1998) and for the most part result in errors of at most one to two dB.

Perhaps the greatest uncertainty arises from the assumption concerning the distribution of the power spectral density for the water vapor fluctuations. If the assumption is incorrect, i.e., if there is some sink or source of water vapor fluctuations within this scale, the $11/3$ power law for the wavelength dependence of the Bragg scatter is not valid. Specifically, if the slope of the power spectral density for water vapor is steeper than $-5/3$, pure Bragg scatter results in a difference greater than 19 dB for the two wavelengths. For a more level slope, differences would be less than 19 dB with a limit of 10 dB if the slope is zero. In the data set analyzed herein, the maximum differences between measurements at S- and X-band varied from 18 to 21 dB, indicating the $-5/3$ assumption is reasonable (Knight and Miller, 1998).

The uncertainty associated with determining Z_R depends on the difference in equivalent reflectivity factors measured at both wavelengths. If Rayleigh scattering

Table 1
Dominant scattering component

Differences in Z_e ($Z_S - Z_X$ in dB)	X-band	S-band
< 3	Rayleigh	Rayleigh
3 to 6	Rayleigh	Neither
6 to 13	Rayleigh	Bragg
13 to 18	Neither	Bragg
> 18	Bragg	Bragg

dominates at X-band, the uncertainty is small. Uncertainty becomes larger (a few dB) if neither scattering mechanism dominates, and becomes very large if Bragg scatter dominates at both wavelengths. For the clouds presented in this study, these uncertainties are small for $Z_X > -10$ dBZ$_e$. For Z_X between -10 and -15 dBZ$_e$ uncertainties are roughly a few dB. For values less than -20 dBZ$_e$ uncertainties become quite large. These values agree qualitatively with estimates of thresholds quoted for similar clouds by Knight and Miller (1993).

2.2. Airborne radar measurements

Data from the Wyoming Cloud Radar (WCR) are used extensively in this study. Pazmany et al. (1994) and Vali et al. (1995) describe prototypes of this radar, flown on the King Air in 1992 and 1994. Characteristics of the WCR relevant to the work presented herein are a 0.7° beam-width, 30 m range resolution, and -18 dBZ$_e$ minimum detectable signal (MDS) at 1 km. The WCR is able to provide a two dimensional cross-section of both reflectivity and Doppler velocity along either a vertical plane (extending upward from the flight level) or a horizontal plane (extending to the right of the flight path). All of the data presented in this study were collected in up-looking mode.

Vertical velocities from the WCR [1] are corrected for aircraft motion through a method described by Leon and Vali (1998). Comparisons of velocities in the nearest usable range gate (roughly 150 m) with aircraft measured winds show the two agree to within roughly 2 m s^{-1}.

Deviations in pitch and roll throughout cloud penetrations were normally less than 5°, resulting in errors in vertical velocities less than 1%. Vertical velocity measurements were not corrected for variations in pitch and roll.

Ground calibrations were conducted, on average, every other day. A trihedral corner reflector with known radar cross-section was used to calibrate the signal output from the receiver. Variations in the calibration were quite large, ± 5 dB for cases in which things were behaving properly. Much of the variation may be traced to problems such as placement of the corner reflector, backscattered power from the 4.5 m high pole on which the corner reflector was mounted, high humidity during the calibrations, and high temperatures in the King Air cabin during the calibrations. Calibrations conducted under more ideal conditions a few weeks after SCMS resulted in variations of only ± 2 dB (Vali et al., 1998).

Radar operating conditions during flights in SCMS were more favorable than during the ground calibrations. Cabin temperatures were lower and humidity was less so that in-flight calibration was more stable. The absolute calibration is accurate to within a few dB, with much greater precision over shorter data segments (tens of minutes).

[1] We refer to these measurements simply as vertical velocities and ignore contributions due to particle fall-speeds. Calculations of reflectivity factors based on measurements from probes mounted on the King Air reveal that nearly all of the backscattered power may be attributed to particles with diameters less than 200 μm. Errors resulting from ignoring the reflectivity weighted terminal fall-speed of these particles is less than 1 m s^{-1}.

2.3. CP-2 and WCR reflectivity comparisons

Direct comparisons were made between CP-2 and WCR measurements. Measurements from both instruments were interpolated onto a common grid within a vertical plane defined by the flight path of the King Air. Grid points were equally spaced, horizontally and vertically, at 35 m.

Data from CP-2 were of lower spatial resolution than the grid and therefore a linear interpolation scheme was used to determine the reflectivity at each grid point. Each interpolated value was the linearly weighted average of the three nearest values, using distance from the grid point as the weighting parameter.

The WCR measurements had considerably higher resolution than the grid. On average, there were six WCR measurements for each grid point. The mean of all of the WCR measurements nearest a given grid location was calculated. This value was then assigned to that grid point.

The interpolation/averaging was done with the reflectivity factors in linear scale (as $mm^6\ m^{-3}$). All values below a threshold were assigned a small, non-zero value representative of the noise. After gridding, values were converted back to log scale.

Comparisons were done for 10 penetrations in 3 clouds on 5 August. The time difference between penetrations and CP-2 volume scans was as large as 120 s. The location of a cloud on the grid plane thus had to be adjusted accounting for advection during this period. The altitude of the King Air for all of the penetrations on 5 August was 1.62 km.

Fig. 2 shows images of reflectivity from CP-2 and the WCR for one penetration through a cloud on 5 August. General characteristics such as cloud size and echo top height from the two data sets compare favorably. In general, echo top heights from the CP-2 and WCR measurements are within ± 60 m. Measurements of echo diameter at any given level also agree to within a few grid-points (roughly 100 m).

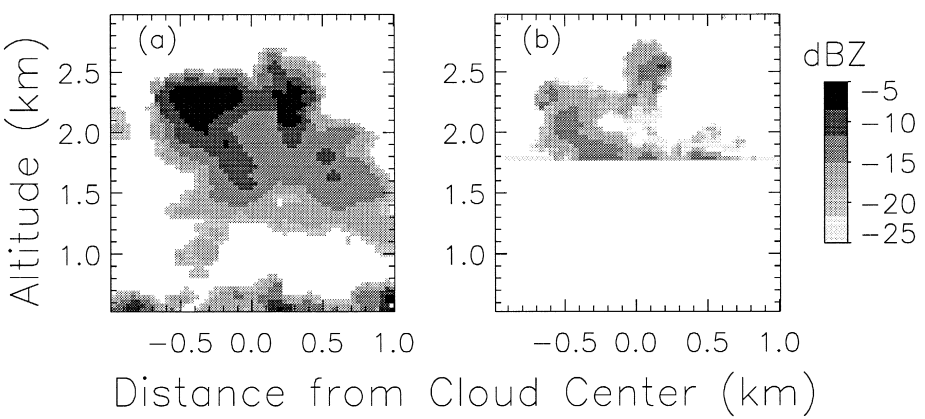

Fig. 2. Reflectivity images from the (a) CP-2 radar and the (b) WCR. The data have been interpolated onto a common grid with a horizontal and vertical resolution of 35 m. The first usable range gate from the WCR is located at 150 m above flight level, roughly 1.8 km.

Direct comparisons of the magnitude of reflectivity measurements were not nearly as good. Fig. 3 shows scatter plots of reflectivity from CP-2 and the WCR. In some instances, there appeared relatively good correlation between the two data sets, with correlation coefficients as large as 0.76. Still, at other times there seemed to be virtually no correlation. In general, the correlation was worse for instances with longer time between the CP-2 volume scan and the King Air penetration. It follows that this decrease in correlation was due to evolution of the reflectivity echo during this period.

For cases where there was reasonable correlation ($\rho > 0.5$) the CP-2 measurements were on average 3 to 5 dB larger than the WCR measurements. Although difficult to pin down exactly, this appeared to be a bias indicating that the absolute calibration of one or both of the radars was in error by a total of roughly 4 dB.

The clouds on 7 August were located 5 to 15 km farther from CP-2, than on 5 August. Also, King Air penetrations in relation to CP-2 were made across range. These factors lead to a much worse resolution of the CP-2 data along the grid plane defined by the King Air flight path. Also, reflectivity factors were on average 5 dB less on 7 August. Therefore, no direct comparisons were made for data from 7 August.

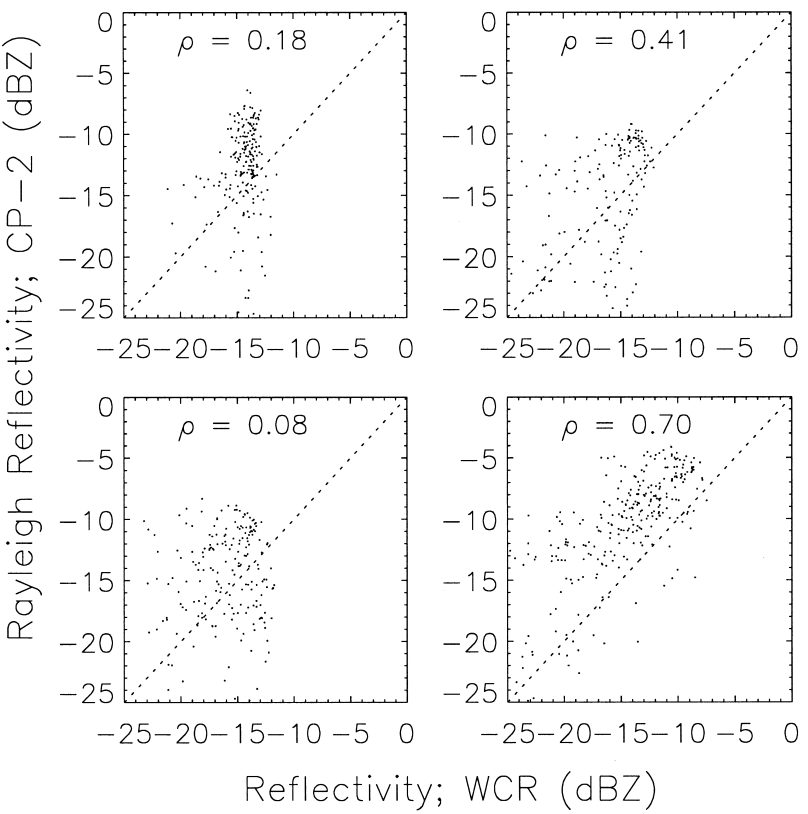

Fig. 3. Scatter plots of measured Rayleigh reflectivity factors from CP-2 and WCR for 4 penetrations in clouds on 5 August. Also shown are the correlation coefficients calculated from measurements during each penetration.

3. General observations

On both days, convection was initiated along a sea breeze front extending north to south, 5 to 20 km east of the CP-2 radar site. Cloud base on both days was roughly 950 m MSL with a temperature of 21°C. Subsidence inversions were located at 1.5 and 2.0 km MSL on 7 August and 5 August, respectively. Cloud tops extended to between 2.5 and 3 km MSL, well above the levels of the inversions. Cloud movement was consistent with the environmental wind at midlevels, northwesterly on 5 August and westerly on 7 August. The convective available potential energy (CAPE) was roughly 700 J kg^{-1} on 5 August and 300 J kg^{-1} on 7 August, indicative of only weak to moderate convection.

On both days winds from the surface to 3 km were light, generally less than 7 m s^{-1}. Shear from cloud base to 2.5 km was weak, on the order of 10^{-3} s^{-1}.

On 5 August, winds below cloud base were southeasterly, onshore, while on 7 August winds were westerly, offshore. Measurements provided by the Desert Research Institute CCN spectrometer (Hudson, 1989) mounted on the NCAR C130 revealed significant differences in CCN concentrations measured just below cloud base on the two days. Ultimately there was a factor of nearly 2.5 difference in cloud droplet concentrations with observed maxima of roughly 350 cm^{-3} on 5 August and 870 cm^{-3} on 7 August. The evolution of the droplet spectra was affected in a predictable fashion. On 5 August droplets growing through condensation achieved much larger sizes than did droplets observed on 7 August for similar levels in cloud (F99). Eventually this resulted in more efficient production of drops with diameters between 50 and 200 μm due to growth by coalescence. F99 concluded that the rapid development of such large droplets through coalescence only occurred after cloud droplets growing through condensation exceeded 40 μm in diameter. Such cloud droplets were observed only in the clouds on 5 August.

4. Cloud evolution

4.1. Qualitative assessment of growth pulses

Fig. 4 shows the evolution of the radar reflectivity factor for one cloud on 5 August. The location of the center of the cloud was determined by interpolating between the locations at the times of the first and last volume scans, from which the direction and speed of cloud movement was calculated. Cross-sections were compiled from 9 volume scans conducted over a period of roughly 20 min. Each cross-section was constructed by interpolating the radar data onto a grid plane defined by the location of the cloud's center and its direction of movement. The arrows indicate the calculated location of the center of the cloud at the time of each volume scan.

The cloud depicted in Fig. 4 experienced 2 pulses of growth. Each pulse resembles a bubble rising through the boundary layer. In the first scan (153315 GMT) there was one bubble, located at roughly 1.5 km MSL (hereafter, all times will refer to Greenwich Mean Time and all altitudes to Mean Sea Level). Two minutes later, it had ascended to roughly 2 km, while another bubble formed to the northwest (left) of the cloud's center.

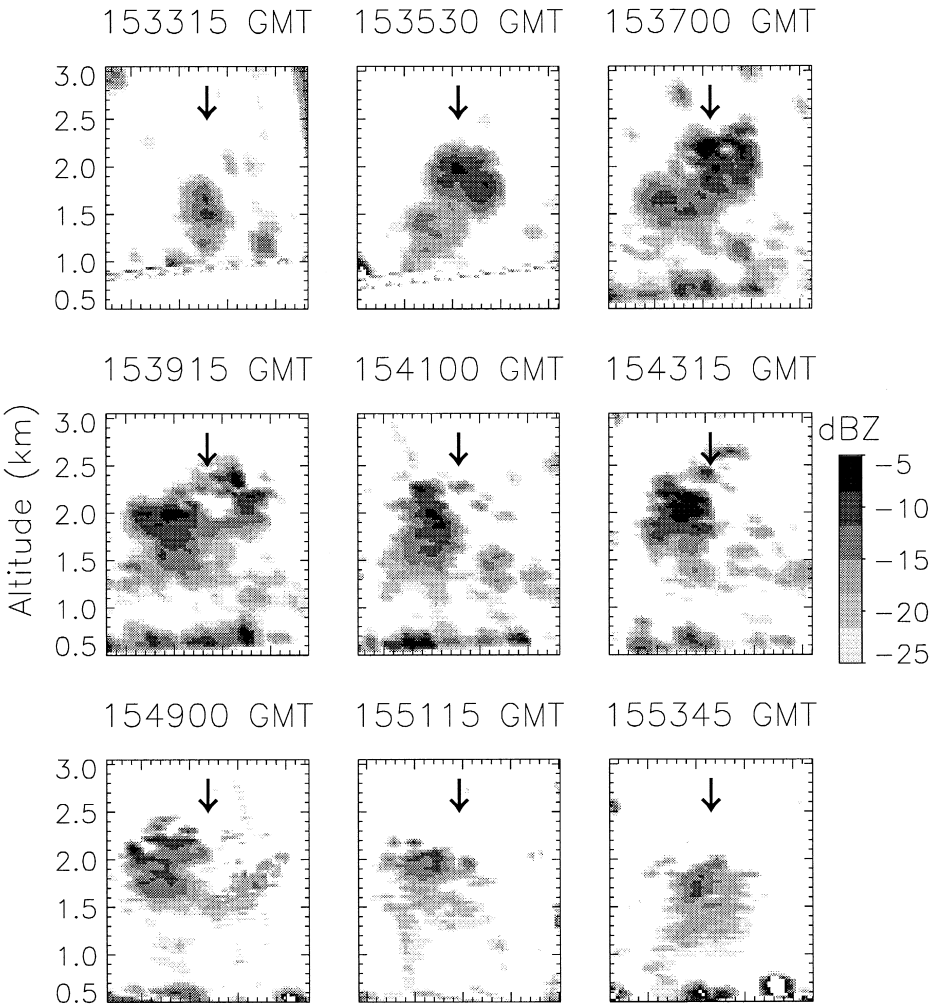

Fig. 4. Vertical cross-sections of reflectivity from CP-2 constructed along the line of motion for cloud C9 on 5 August. The arrow shows the location of the cloud center. Major tick-marks are at 0.5 km.

The altitude of the new bubble was between 1 and 1.5 km. Over the next few minutes, the initial pulse continued to rise and break apart as it penetrated further into the dry air within and above the inversion. At the same time, the second pulse ascended through the remnants of the first. The second pulse achieved a higher altitude and slightly greater reflectivity than did the first pulse. Also, the last few volume scans reveal a reflectivity echo (-20 to -15 dBZ) extending downward from the base of the cloud.

Fig. 5 shows vertical cross-sections of radar reflectivity over a period of 22 min for another cloud on 5 August. This cloud also experienced multiple growth pulses throughout its lifetime. Yet, unlike the cloud shown in Fig. 4, the pulses do not resemble individual bubbles but rather appear more as a reflectivity echo pulsating over time.

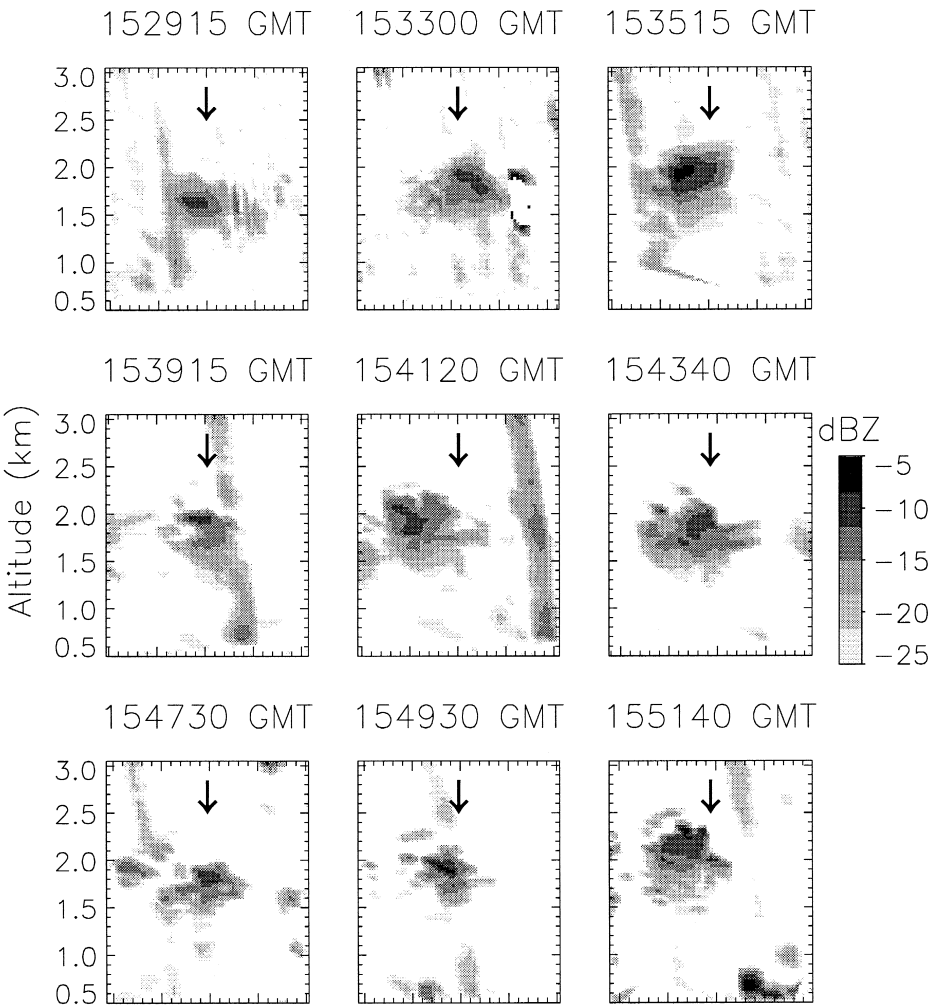

Fig. 5. As in Fig. 4 except for cloud C8 on 5 August.

During the first 6 min (3 volume scans) the cloud was growing. During this period, the altitude of the echo top increased, as did the maximum reflectivity. Between 153515 and 153915, the cloud decayed somewhat before experiencing reinvigorated growth up until 154340. The cloud experienced one final pulse of growth between 154730 and 155140. After which it decayed in a period of 4 to 5 min.

The UW King Air made 6 penetrations at 1.6 km through the center of the cloud shown in Fig. 5. The first penetration was made at 153315, the last at 155515. Cross-sections of reflectivity and vertical velocity from the WCR for all 6 penetrations are shown in Fig. 6. Over the first two penetrations (153315 to 153640) the cloud was growing. The echo top height increased and vertical velocities were mostly positive during both penetrations. The cloud edge was well defined and the echo was quite

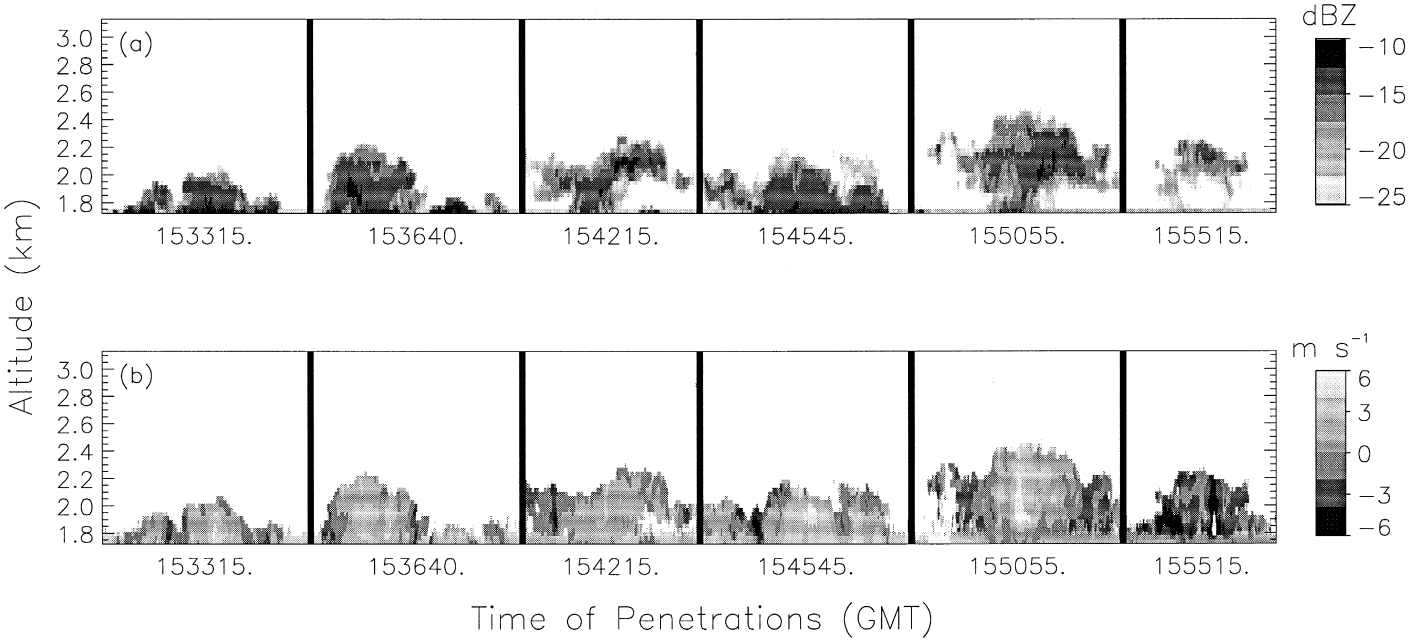

Fig. 6. Vertical cross-sections of (a) reflectivity and (b) vertical velocity from the WCR for 6 penetrations made in cloud C8 on 5 August. The scale is such that there is a 1:1 aspect ratio between the vertical and horizontal dimensions.

compact. By the third penetration (154215) the vertical velocities had weakened somewhat. The cloud edges had become less well defined and the cloud appeared to be breaking apart. A few minutes later, at 154545, the echo top height had decreased. Positive vertical velocities were once again found throughout much of the cloud. The cloud edge was well defined and the cloud appeared to be growing. Measurements made during the fifth penetration (155055) revealed that, although there was still a significant area of positive vertical air motion, the echo was breaking apart and appeared to be reaching the maximum growth for this pulse. Finally, during the last penetration (155515) the cloud was composed entirely of downward moving air and was well into its decay stage.

4.2. Further evidence of pulsating growth

The data presented in Figs. 4–6 are representative of the observations obtained from all of the clouds on both days. The images provide a qualitative interpretation of the growth of the clouds, but do not supply adequate information for a more rigorous quantitative evaluation. For this, it is necessary to reduce the radar measurements to quantitatively describe the essentials of the growth pulses (e.g., growth in echo top height, increase in maximum reflectivity).

Fig. 7 shows time–height cross-sections of the Rayleigh reflectivity factor reconstructed from measurements made by CP-2 for the 6 clouds on both days. The diagrams show the minimum and maximum altitude of reflectivity contours ranging from −20 to −5 dBZ at 5 dB intervals. In constructing the cross-sections, entire cloud volumes from each radar volume scan were considered in determining the minimum/maximum height for each contour at the time of that scan.

For all of the clouds the level at which a given reflectivity echo formed was roughly the same. The −15 dBZ echo formed at roughly 1.2 km and the −10 dBZ echo at 1.5 km. For the clouds on 5 August, the −5 dBZ echo formed at 2 km, on 7 August it formed at 2.4 km. All of the clouds on 5 August achieved reflectivity factors exceeding −5 dBZ, only 1 cloud achieved this on 7 August

In nearly all cases, the minimum altitude for given reflectivity contours remained at roughly the same level throughout a cloud's lifetime. The one exception to this was cloud C9. The descent of the −20 and −15 dBZ echo for cloud C9 (also seen in Fig. 4) was due to the development and eventual settling of precipitation. Flight scientists on both the King Air (at midlevels) and the C130 (near cloud base) noted drizzle during the later penetrations of this cloud (F99).

For all of the clouds the overall evolution of the reflectivity echoes was quite similar and consistent with the interpretation of the images provided both by the CP-2 radar and the WCR. The evolution of individual clouds consisted of 2 to 3 growth pulses lasting from 5 to 10 min. The growth of the pulses may be tracked through increases in the height of the cloud echo top. From this it follows that while the echo top height was increasing, the pulse was growing. The growth phases of individual pulses were separated by lulls in the ascent of the echo top. Further, for two of the clouds on 7 August, growth phases were separated by a period of rapid descent of the echo top.

On 5 August, the altitude achieved by individual pulses was greater for subsequent pulses within the same cloud. This behavior was only observed in one cloud on

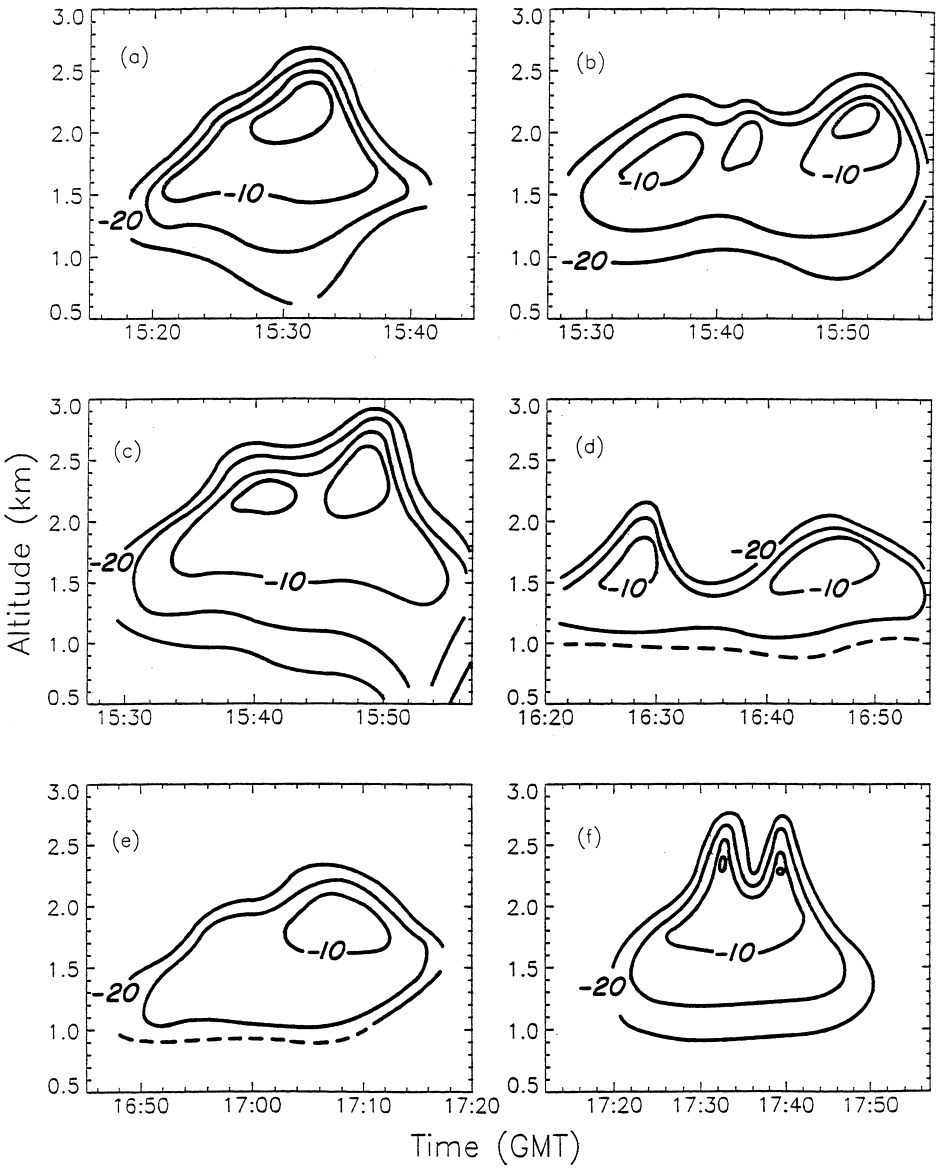

Fig. 7. Time height cross-sections of reflectivity. Observations were made in 3 clouds on 5 August: (a) C5, (b) C8, and (c) C9; and in 3 clouds on 7 August: (d) C1, (e) C4, and (f) C10. The measurements are from CP-2 and represent the maximum/minimum height of reflectivity contours throughout the entire cloud at given times. Contour intervals are every 5 dB.

7 August. This difference is related to the amount of decay between pulses, which is ultimately tied to the moisture content within and above the inversion on the two days.

We define the growth rate for individual pulses as the rate of ascent of the maximum height of a given reflectivity contour. For this, the −15 dBZ contour is chosen, arbitrarily. The calculated growth rate for pulses in clouds on 5 August was between 1.3 and 2.8 m s^{-1}, and between 1.3 and 5.2 m s^{-1} for clouds on 7 August. For all clouds the growth rates were less, roughly by a factor of 2, than the maximum observed vertical velocities.

Table 2 lists characteristics for all of the pulses in the 6 clouds on both days. Included in the table are the number of pulses associated with each cloud, the altitude at which the −15 and −10 dBZ echo formed, the average growth rate for each pulse, the maximum altitude achieved by the −15 dBZ echo, and the maximum reflectivity within that pulse.

4.3. WCR measurements and reflectivity flux

From the WCR measurements it is possible to relate the growth and decay of pulses to the vertical velocity field within a cloud. But, the low temporal resolution of the WCR data set coupled with the relatively short life cycle of individual pulses makes it rather difficult to determine a one-to-one correspondence between pulses and the kinematic evolution of the clouds. Thus, the overall evolution so apparent in the CP-2 data set is difficult to determine from the WCR measurements. This was overcome by defining a quantity used to track pulses within the WCR data. This quantity we call the reflectivity flux.

The reflectivity flux is calculated by multiplying the vertical velocity with the reflectivity factor, both measured from the WCR, and having units of mm^6 m^{-2} s^{-1}. The sign of the reflectivity flux is determined solely by the sign of the vertical velocity;

Table 2
Observed characteristics of pulses

Date cloud	Pulse	Alt.[a]—15 dBZ (km)	Alt.[a]—10 dBZ (km)	Max Alt.—15 dBZ (km)	Growth rate (m s^{-1})	$MaxZ_e$ (dBZ)
5 Aug						
C5	1	1.2	1.5	2.2	2.78	−7
	2	1.2	1.5	2.65	1.74	−3
C8	1	1.2	1.6	2.15	1.56	−8
	2	1.3	1.7	2.2	1.45	−8
	3	1.2	1.65	2.45	1.39	−4
C9	1	1.2	1.5	2.5	2.38	−4
	2	1.1	1.5	2.85	1.36	−2
7 Aug						
C1	1	1.1	1.5	2.05	2.22	−8
	2	1.1	1.5	1.95	1.60	−9
C4	1	1.1		1.95	1.98	−11
	2	1.1	1.6	2.2	1.39	−7
C10	1	1.2	1.65	2.7	3.78	−5
	2	1.2	1.65	2.65	5.20	−5

[a] This altitude refers to the level at which the given echo formed.

while the magnitude depends on both the magnitudes of the vertical velocity and the reflectivity factor.

The reflectivity flux is the vertical flux of the reflectivity factor, or, in more general terms, the flux of the sixth moment of the droplet spectrum. In this respect, it is similar to the oft-quoted liquid water flux (third moment of the droplet spectrum).

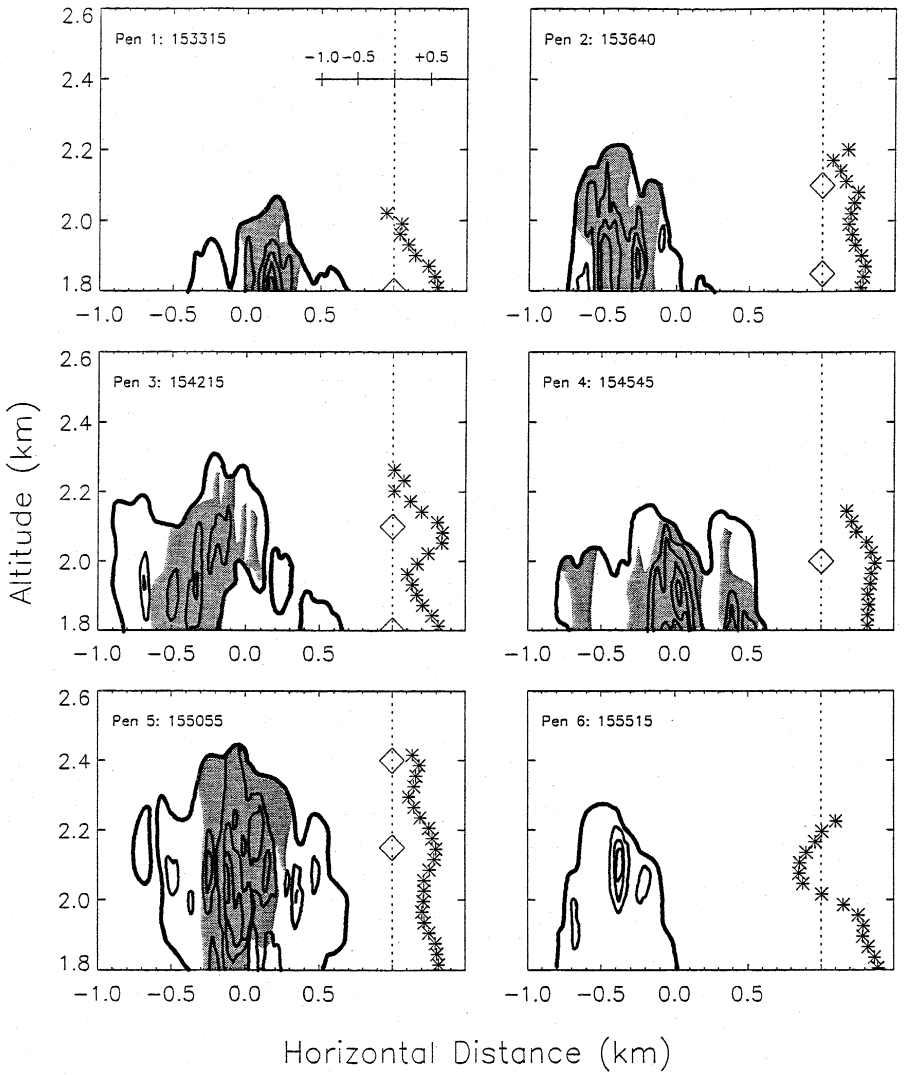

Fig. 8. Contours of reflectivity flux for 6 penetrations of cloud C8 on 5 August. The contour levels are 0.05 $mm^6\ m^{-2}\ s^{-1}$. Stippled regions denote areas of positive reflectivity flux. The thick solid line outlines the −25 dBZ echo contour from the WCR. Asterisks on the right side of each plot represent the correlation between reflectivity and vertical velocity for each level. The scale for these graphs is shown at the top of the upper most left plot. Diamonds indicate the levels of pulses based on reflectivity flux and local maxima within the correlation plots.

In general, the flux of a conservative quantity is related to the convergence/divergence of that quantity and the resulting advection through a unit surface. Because the reflectivity factor is not a conserved parameter, either the creation or destruction of reflectivity through the growth or evaporation of droplets may also affect the flux. Thus, the relationship between the reflectivity and velocity that is described by the flux depends on both the advection and sources/sinks of reflectivity.

Fig. 8 shows contours of reflectivity flux for 6 penetrations made in one cloud on 5 August. Contour intervals are 0.05 $mm^6\ m^{-2}\ s^{-1}$. Also, regions where the reflectivity

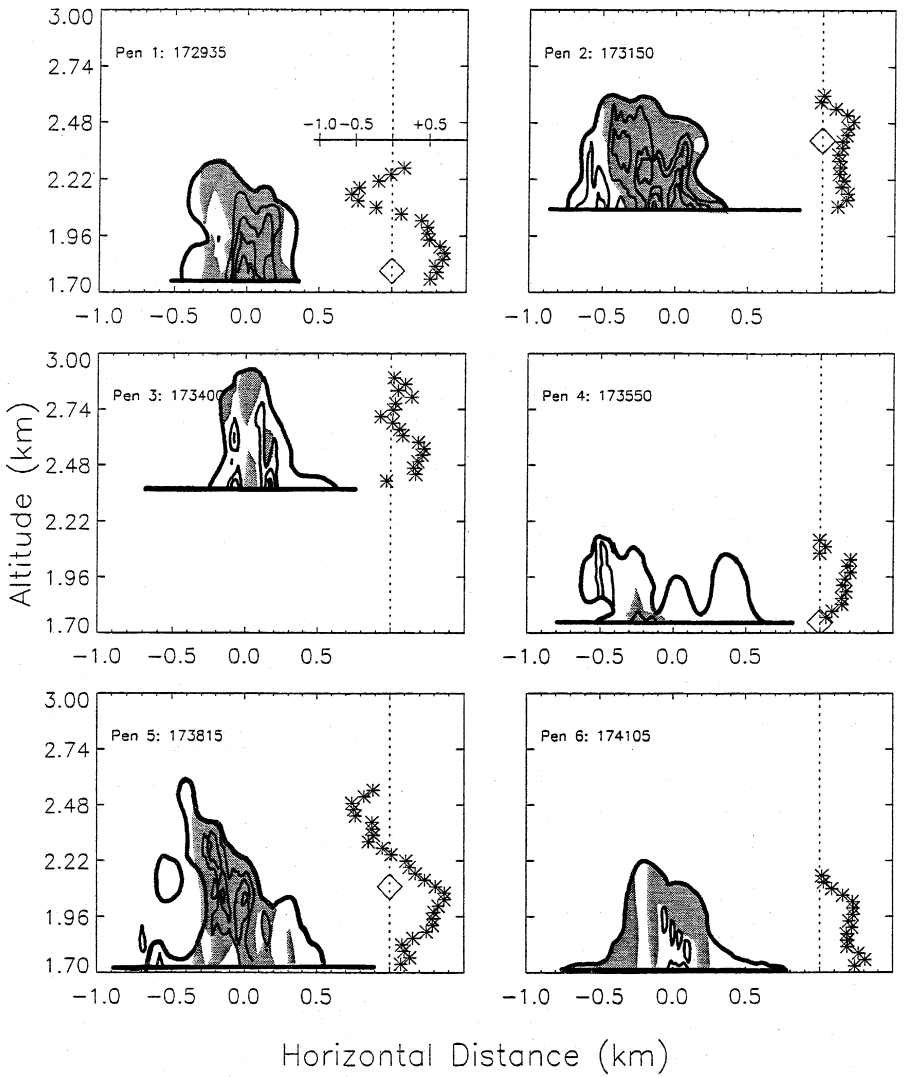

Fig. 9. As in Fig. 8 except for cloud C10 on 7 August.

flux is positive are shaded. Areas of reflectivity flux greater than roughly 0.05 $mm^6\ m^{-2}\ s^{-1}$ appear as bubbles within the cloud. Also shown are values of the coefficient of correlation between the reflectivity factor (in dBZ) and the vertical velocity, calculated for each range gate.

In general, correlation coefficients show a local maximum at levels where large positive reflectivity flux occurs. Such areas are indicative of bubbles. Bubbles appear as cloud scale features. There often exists significant variation in reflectivity flux within individual bubbles. Although the variations within individual bubbles are highly transient features, the bubbles themselves are not and they may be tracked as they ascend using data of relatively low temporal resolution.

The altitude for which there exists large correlation and reflectivity flux (denoted by a diamond in Fig. 8) is plotted as a function of time in Fig. 10a. The dashed line connecting these points represents the ascent of individual bubbles. The top of the −15 dBZ echo contour from the CP-2 data (as shown in Fig. 7) is overlaid for reference. For all three pulses, the ascent of the bubbles depicted from the measurements provided by the WCR match the observations from the CP-2 data.

Results from a similar analysis of measurements made during six penetrations between 1.5 and 2.2 km of a cloud on 7 August are shown in Figs. 9 and 10b. Bubbles outlined in the reflectivity flux can again be tracked throughout the evolution of the cloud from the altitude of maxima for the coefficient of correlation between reflectivity and vertical velocity. The first pulse is sampled during the first and second penetrations. The second pulse was sampled during the fourth and fifth penetrations. The growth rates indicated from the WCR measurements agree extremely well with those calculated independently from the CP-2 data set.

The signature of the decay of pulses can also be seen in plots of correlation versus altitude. In Fig. 8 during the sixth penetration, there was a region of negative correlation above 2 km. This corresponds to a time of rapid decay as indicated from CP-2 measurements. Likewise, in Fig. 9, during the first penetration above the level of the

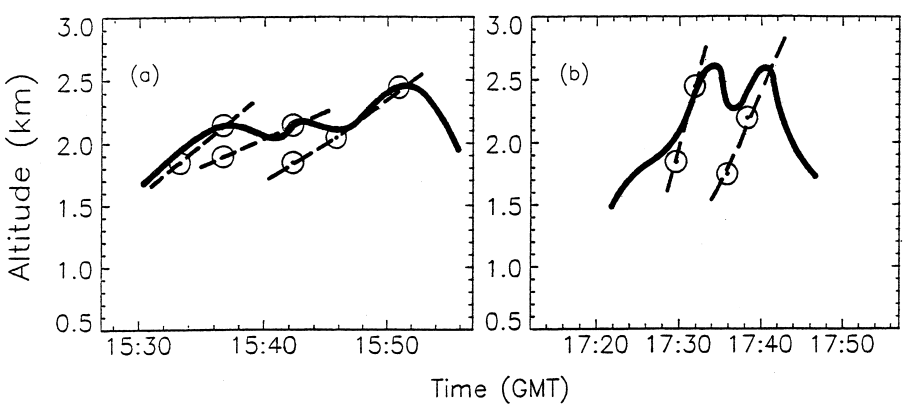

Fig. 10. Plots showing the level of pulses for (a) cloud C8 deduced from Fig. 8, and for (b) cloud C10 deduced from Fig. 9. Dashed lines connect the same pulse and represent the ascent rate of that pulse. For comparison, the −15 dBZ echo top contour from CP-2 measurements is also shown.

first growth pulse, a strong negative correlation most likely corresponds to the decay of an earlier pulse from the remnants of another cloud.

The values of both reflectivity flux and correlation coefficients were comparable for all clouds in this study. In general, bubbles were defined as regions of positive reflectivity flux, greater than 0.05 $mm^6\ m^{-2}\ s^{-1}$. Maxima in the correlation coefficients were roughly 0.5 to 0.8; minima were between -0.3 and -0.5.

5. Discussion

The pulsating nature of growth of clouds observed during SCMS is consistent with numerous studies describing the growth of cumulus clouds either as individual bubbles or a collection of multiple bubbles (e.g., Ludlam and Scorer, 1953; Saunders, 1961; Blyth et al., 1988; Barnes et al., 1996). Our results simply reinforce the theory of bubble growth for cumuli.

5.1. Summary of cloud evolution

The evolution of clouds observed in this study can be best represented by a collection of 2 to 3 pulses defined by a cycle of growth followed by decay. In general, there was only one pulse occurring at any given time during a cloud's evolution. Individual pulses lasted roughly 10 to 15 min. During this period the growth/decay of a pulse could be tracked with the aid of data from the CP-2 and WCR.

The growth phase of a pulse was clearly identifiable within the CP-2 data set by a rapidly ascending echo top. During the growth period, the vertical flux of the reflectivity was positive throughout much of the cloud. The region of positive reflectivity flux often resembled a bubble rising through the boundary layer. Near the level of the maximum flux there was a strong correlation between vertical velocity and the reflectivity factor indicating the highest reflectivity factors were collocated with the core updraft. As individual bubbles continued to ascend, the value of the associated maxima in the correlation coefficients decreased slightly.

When a pulse reached the end of its growth stage, the ascent rate of the cloud echo top decreased to zero. Images from the WCR for pulses at this stage reveal a much less well-defined echo edge and reduced vertical velocities. The correlation between the reflectivity and vertical velocity was less than during the growth phase as was the peak value of the reflectivity flux.

Decay of pulses was characterized by periods of decrease in echo top height along with negative reflectivity flux. In general, there was a strong negative correlation between the reflectivity and vertical velocity during the decay phase. On 5 August, only the final pulse of a cloud experienced any noticeable decay while nearly all of the pulses for clouds on 7 August went through this stage. This was most likely due to the drier environment on 7 August leading to mixed parcels in which greater evaporation occurred. Ultimately this resulted in greater negative buoyancy and greater decay.

The picture presented of the growth and decay of individual bubbles is quite similar, at least schematically, to results from the modeling studies of Klaassen and Clark

(1985). These studies, further extended by Grabowski and Clark (1991, 1993), employed a high-resolution grid to explicitly model entrainment/detrainment events and their effects on cloud evolution. Extensive regions of adiabatic liquid water content (LWC) and a cloud with smooth, well-defined top and sides characterize model predictions of early cloud growth. After roughly 8 to 10 min, nodes begin forming along the cloud/clear air interface at the top and sides of the modeled clouds. Klaassen and Clark attribute the development of the nodes to instabilities arising from density differences across the interface. As these nodes continue to grow, cloudy air is detrained into the environment while at the same time sub-saturated air is entrained into the cloud as discrete parcels. Eventually the cloud/clear air interface breaks down and the resulting LWC field looks remarkably similar to images from the WCR presented earlier for clouds reaching the maximum growth stage of a pulse.

When compared with measurements from the WCR, vertical velocity fields also looked quite similar throughout the entire evolution of the modeled clouds. Early in the evolution of the modeled clouds, vertical velocities are nearly all positive, with maxima occurring near the center. As nodes develop and the cloud/clear air interface breaks down, the modeled vertical velocity field becomes highly distorted and again looks quite similar to measurements from the WCR.

It seems reasonable that the decay of the pulses within the observed clouds is related to entrainment/detrainment of environmental and cloudy air. Grabowski (1993) concluded that descending volumes of air in and around convective bubbles are the result of entrainment leading to buoyancy reversing plumes. He found that the main effect of buoyancy reversal was to increase the intermittence associated with cloud evolution, leading to variations in cloud top height and maximum/minimum vertical velocities with time. His findings, based on results from a numerical model of two fluids with different densities, are again similar to the observations described in this study.

5.2. Development of reflectivity echoes

The evolution of the Rayleigh reflectivity echo in relation to the vertical velocity field was closely tied to the pulsating nature of growth of a given cloud. In particular, during the growth phase, the strongest reflectivity was in the updraft, while during the decay phase the greatest reflectivity was often found in the downdraft. This switch in the relationship between the reflectivity factor and vertical velocity was related to what particles were actually dominating the reflectivity at a given period in a cloud's evolution.

In studies of similar clouds from SCMS, Knight and Miller (1998) argued that under certain conditions measurements from CP-2 revealed cloud droplets growing through condensation during adiabatic ascent. Evidence provided included plots of measured reflectivity as a function of altitude. From this, they noted that the maximum values of the reflectivity factors at a given level matched reasonably well with those calculated from an uni-modal, symmetric distribution of cloud droplets growing through condensation, assuming adiabaticity and realistic cloud base conditions. Anecdotal evidence also included the existence of flat echo bases particularly during the growth phase, both spatially (from individual volume scans) and temporally (within time–height cross-sections).

We too find flat echo bases for reflectivity factors between −15 and −10 dBZ, particularly in growing clouds (i.e., Figs. 4 and 5). F99 calculated reflectivity factors from in situ measurements of cloud droplets (diameters less than 50 μm) at various levels for clouds on both days. Their findings suggest that on both days, at 1.2 km, the maximum reflectivity due solely to cloud droplets was roughly −19 dBZ. CP-2 measurements from both days revealed that this was the level at which the −15 dBZ Rayleigh echo formed. At 1.6 km, the level at which the −10 dBZ echo formed, maximum calculated reflectivity factors were −13 dBZ for clouds on 5 August and −17 dBZ on 7 August.

From the data presented in Section 2.3, a difference of roughly 4 dB between the CP-2 and WCR measurements was noted. If indeed the CP-2 calibration was high by this amount it could account for some of the difference between the measured and calculated values. Another possible explanation for this discrepancy is that some portion of the reflectivity echo was likely due to drops with diameters greater than 50 μm. Although this is unlikely for the lower regions (below roughly 1.5 km), at mid-levels and above, in situ measurements indicated the reflectivity due to such drops was on average roughly equal to the reflectivity from the smaller cloud droplets (F99). Further, these drops showed a slight tendency to occur in regions of moderate to strong updraft, precisely the location that the greatest reflectivity echoes are found in the growing clouds.

A very puzzling aspect of the data is that the level at which the −10 dBZ echo formed was the same for clouds on 5 August and 7 August. In situ measurements indicated there should be a difference of somewhere between 300 and 500 m, with the echo forming at higher levels on 7 August. On 7 August, the air within the inversion was considerably drier, resulting in stronger Bragg echoes. The uncertainty for determining a value for a given Rayleigh reflectivity echo was therefore larger on 7 August. Still, the uncertainty would be even greater for weaker echoes. At the same time, the Bragg echo is stronger at midlevels and above. This may account for the above noted discrepancy, but the evidence is only speculative.

The development of drops with diameters in excess of 50 μm was evident in the WCR measurements as pulses reached their maximum growth and began to decay. The maximum reflectivity through these stages was no longer located within the strongest updrafts, but instead occurred either with no preferential location (zero correlation) or in regions of downdraft (negative correlation). Measurements of droplet spectra within regions of weak or downward moving air indicate flat spectra with a reduced concentration (F99). Correspondingly, the reflectivity due to cloud droplets in these regions would also be significantly reduced. Yet, in many instances, measurements from the WCR reveal still quite strong reflectivity. Therefore, the reflectivity in such regions must have been the result of scattering from larger drops.

6. Concluding remarks

The observations reported here have provided the first glance into the very early development of the Rayleigh reflectivity echo and structure of the vertical velocity field

in small cumuli. To interpret the development of reflectivity echoes and their relationship to vertical velocity it is necessary to understand not only how cloud droplets and drizzle drops are distributed (discussed in F99) but also understand the overall evolution of the cloud. We have demonstrated the importance of pulsating growth as it relates to both the evolution of reflectivity echoes and to which size particles dominate the reflectivity at given times and locations in cloud.

This data set has demonstrated that growth of droplets through condensation can be seen from radar measurements. But, to distinguish between regions of cloud droplets growing through condensation and larger drizzle drops it is important to know the phase of growth of the cloud. Such discrimination should also require measurements of vertical velocity. In general, for growing pulses, high reflectivity factors collocated with strong updrafts are at least in part, if not completely, the result of scattering by cloud droplets. In regions of weak vertical motion, especially during decay, higher reflectivity factors are most certainly due to larger drops.

The growth and decay of individual pulses and therefore the overall evolution of the cloud is intimately tied to entrainment/detrainment. This in turn depends at least in part on the moisture content of the environment. For clouds that develop in an environment containing less moisture within and above the inversion there was greater decay between pulses. In this case, the growth of earlier pulses did not significantly affect the evolution of later pulses. But, when there was considerably less decay between pulses (e.g., 5 August) subsequent pulses were able to grow higher and produce stronger reflectivity echoes. This indicates the importance of environmental preconditioning through the successive growth of bubbles.

Acknowledgements

We would like to thank Bob Rilling and NCAR/ATD for supplying us with the CP-2 data. We also thank Brad Baker for discussions relating to Bragg scattering and the separation of the Bragg and Rayleigh components of the total backscatter. David Leon played an instrumental role in the processing of data from the WCR. Susan Allen drafted many of the figures. We gratefully acknowledge Samuel Haimov and the rest of the crew at UW for their tireless effort during and after SCMS. This work was supported under NSF grants ATM-9319907 and ATM-9712859.

References

Atlas, D., 1959. Meteorological angel echoes. J. Meteorol. 16, 6–11.

Austin, P.H., Baker, M.B., Blyth, A.M., Jensen, J.B., 1985. Small-scale variability in warm continental cumulus clouds. J. Atmos. Sci. 42, 1123–1138.

Barnes, G.M., Fankhauser, J.C., Browning, W.D., 1996. Evolution of the vertical mass flux and diagnosed net lateral mixing in isolated convective clouds. Mon. Weather Rev. 124, 2764–2784.

Blyth, A.M., Latham, J., 1985. An airborne study of vertical structure and microphysical variability within a small cumulus. Q. J. R. Meteorol. Soc. 111, 773–792.

Blyth, A.M., Cooper, W.A., Jensen, J.B., 1988. A study of the source of entrained air in Montana cumuli. J. Atmos. Sci. 45, 3944–3964.

Doviak, R.J., Zrnic, D.S., 1984. Doppler Radar and Weather Observations. Academic Press, San Diego, CA, USA.

French, J.R., Vali, G., Kelly, R.D., 1999. Observations of microphysics pertaining to the development of drizzle in warm, shallow cumulus clouds, submitted to Q. J. R. Meteorol. Soc.

Grabowski, W.W., 1993. Cumulus entrainment, fine-scale mixing, and buoyancy reversal. Q. J. R. Meteorol. Soc. 119, 935–956.

Grabowski, W.W., Clark, T.L., 1991. Cloud–environment interface instability: rising thermal calculations in two spatial dimensions. J. Atmos. Sci. 48, 527–546.

Grabowski, W.W., Clark, T.L., 1993. Cloud–environment interface instability: Part II. Extension to three spatial dimensions. J. Atmos. Sci. 50, 555–573.

Hudson, J.G., 1989. An instantaneous CCN spectrometer. J. Atmos. Oceanic Technol. 6, 1055–1065.

Johari, H., 1992. Mixing in thermals with and without buoyancy reversal. J. Atmos. Sci. 49, 1412–1426.

Jonas, P.R., 1990. Observations of cumulus cloud entrainment. Atmos. Res. 25, 105–127.

Klaassen, G.P., Clark, T.L., 1985. Dynamics of the cloud–environment interface and entrainment in small cumuli: two-dimensional simulations in the absence of ambient shear. J. Atmos. Sci. 42, 2621–2642.

Knight, C.A., Miller, L.J., 1993. First radar echoes from cumulus clouds. Bull. Am. Meteorol. Soc. 74, 179–188.

Knight, C.A., Miller, L.J., 1998. Early radar echoes from small, warm cumulus: Bragg and hydrometeor scattering. J. Atmos. Sci. 55, 2974–2992.

Leon, D., Vali, G., 1998. Retrieval of three-dimensional particle velocity from airborne Doppler radar data. J. Atmos. Oceanic. Technol. 15, 860–870.

Ludlam, F.H., Scorer, R.S., 1953. Convection in the atmosphere. Q. J. R. Meteorol. Soc. 79, 317–341.

Mason, B.J., Jonas, P.R., 1974. The evolution of droplet spectra and large droplets by condensation in cumulus clouds. Q. J. R. Meteorol. Soc. 100, 23–38.

Ottersten, H., 1969. Atmospheric structure and radar backscattering in clear air. Radio Sci. 4, 1179–1193.

Pazmany, A.L., McIntosh, R.E., Kelly, R.D., Vali, G., 1994. An airborne 95 GHz dual-polarized radar for cloud studies. IEEE Trans. Geosci. 32, 731–739.

Roesner, S., Flossman, A.I., Pruppacher, H.R., 1990. The effect on the evolution of the drop spectrum in clouds of the preconditioning of air by successive convective elements. Q. J. R. Meteorol. Soc. 116, 1389–1403.

Saunders, P.M., 1961. An observational study of cumulus. J. Meteorol. 18, 451–467.

Szumowski, M.J., Rauber, R.M., Ochs, H.T. III, Miller, L.J., 1997. The microphysical structure and evolution of Hawaiian rainband clouds: Part I. Radar observations of rainbands containing high reflectivity cores. J. Atmos. Sci. 54, 369–385.

Vali, G., Kelly, R.D., Pazmany, A., McIntosh, R.E., 1995. Airborne radar and in situ observations of a shallow stratus with drizzle. Atmos. Res. 38, 361–380.

Vali, G., Kelly, R.D., French, J., Haimov, S., Leon, D., McIntosh, R., Pazmany, A., 1998. Fine-scale structure and microphysics of coastal stratus. J. Atmos. Sci. 55, 3540–3564.